ACS APPLIED MATERIALS & INTERFACES

Research Article

www.acsami.org

# Efficient Delivery of DOX to Nuclei of Hepatic Carcinoma Cells in the Subcutaneous Tumor Model Using pH-Sensitive Pullulan–DOX Conjugates

Huanan Li,[‡] Yani Cui,[†] Junhui Sui,[†] Shaoquan Bian,[†] Yong Sun,*[,†] Jie Liang,[†] Yujiang Fan,*[,†] and Xingdong Zhang[†]

[†]National Engineering Research Center for Biomaterials, Sichuan University, 29 Wangjiang Road, Chengdu 610064, China

[‡]College of Biomedical Engineering, Chongqing Medical University, Yixueyuan Road, Yuzhong District, Chongqing 400016, China

**ABSTRACT:** A series of pullulan–doxorubicin conjugates (Pu-DOXs) were investigated for effectively delivering DOX to nuclei of hepatic carcinoma cells in subcutaneous tumor model. These Pu-DOXs were prepared by conjugating DOX onto pullulan molecule via pH-responsive hydrazone bond using spacers with different alkane chain length. The highest drug loading content of Pu-DOXs went up to nearly 50%, and the diameter of Pu-DOX nanoparticles ranged from 50 to 170 nm, as measured by DLS and TEM. These Pu-DOX nanoparticles could rapidly release DOX in the acidic environment at pH = 5.0 while being kept relatively stable in neural conditions. The in vitro cell coculture experiments revealed that these Pu-DOX nanoparticles were selectively internalized by hepatic carcinoma cells through receptor-mediated endocytosis via asialoglycoprotein receptor on the hepatic carcinoma cell surface. DOX was rapidly released from Pu-DOX nanoparticles in acidic endosome/lysosome, diffused into cell nuclei due to its strong affinity to nucleic acid, inhibited the cell proliferation, and accelerated the cell apoptosis. In the nude mice subcutaneous hepatic carcinoma model, Pu-DOX nanoparticles efficiently accumulated in the tumor site through the enhanced permeation and retention effect. Then DOX was specifically internalized by hepatic carcinoma cells and rapidly diffused into the nuclei of cells. Compared with the control group in in vivo experiments, these Pu-DOX nanoparticles effectively inhibited solid tumor growth, prolonging the lifetime of the experimental animal. These pH sensitive nanoparticles might provide an important clinical implication for targeted hepatic carcinoma therapy with high efficiency and low systematic toxicity.

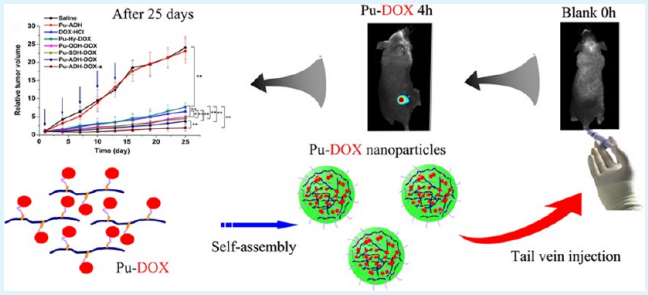


**KEYWORDS:** *pullulan, pH-sensitive, nanoparticles, doxorubicin, hepatic carcinoma*

## 1. INTRODUCTION

Chemotherapy, as one conventional method in tumor treatment, aims to prolong life or to palliate symptoms of malignant tumor sufferers. However, classical chemotherapeutics are prone to randomly distribute in nontarget tissues, and usually easy to be eliminated by renal clearance, leading to the effective drug concentration at the tumor sites far below those required to destroy the solid tumor, and causing serious side effects.[1,2] Thus, there is an insistent demand for the ideal chemotherapy strategy to deliver sufficient levels of chemotherapeutics specifically to tumor sites while not affecting healthy organs and tissues.

Doxorubicin (DOX), as an anthracycline antibiotic, has an obvious inhibition effect on a wide range of cancers. Like all anthracyclines, it works by intercalating DNA, inhibiting macromolecular biosynthesis, and thereby disrupting or blocking the process of cancer cell replication.[3−6] However, various undesired side effects, led by life-threatening heart damage, were reported.[7−9] For reducing the side effects and enhancing the therapeutic efficacy, in recent years, numerous efforts have been undertaken to provide new approaches for targeting drug delivery by nanoparticular carriers.[10−13] The nanoparticles with sufficient stability, proper size, and outstanding surface properties could availably prevent immature drug release in the convection of vasculature circulation before they reach the tumor sites, avoid the rapid filtration by the kidney and clearance by the reticuloendothelial system (RES) and accelerate the drug accumulation at tumor sites through the enhanced permeation and retention (EPR) effect.[14−16] However, efficient cellular uptake of nanoparticles by cancer cells and rapid intracellular drug release play crucial roles in antitumor therapy since DOX mainly acts on the nucleic acids.[17,18] Intelligent nanoparticles, which could rapidly release the loaded drugs in response to specific stimuli in intercellular and extracellular environment of cancer cells, e.g. pH value,[19,20] temperature, enzyme,[21,22] light,[23] and redox condition,[24,25] have been demonstrated to improve the bioavailability of the antitumor drugs. Among them, pH-responsive nanoparticles

Received: April 12, 2015
Accepted: July 3, 2015
Published: July 3, 2015

  

DOI: 10.1021/acsami.5b03150
ACS Appl. Mater. Interfaces 2015, 7, 15855−15865

have attracted great attention because of its mature structure design, universal applicability, and selective biodegradability.[26,27]

Pullulan is a nonionic natural polysaccharide that possesses not only the common features of polysaccharides, such as high biocompatibility, biodegradability, and polyfunctionality for chemical decoration, but also excellent blood compatibility, nonimmunogenicity, and fair solubility in water and a few organic solvents.[28,29] These characteristics provide pullulan with high stability in blood, prevent it from capturing by RES, and elongate the circular life in the vasculature circulation.[30,31] Sharma and his co-workers reported that pullulan derivatives were conduced to prolong the residence period of nanoparticles in blood circulation and enhance the internalization by liver cells through receptor mediated endocytosis.[32] Interestingly, pullulan shows a specific affinity to asialoglycoprotein receptor (ASGP-R), which is specific for hepatocytes, and highly expressed on their sinusoidal membranes.[33] Naturally, ASGP-R recognizes and internalizes glycoproteins with terminal galactose or *N*-acetylglucosamine residues via clathrin-coated pits.[34] Therefore, a specific manner of drug delivery by bound drug to appropriate glycoproteins, lactose, or galactose would provide more significant therapeutic benefits in hepatic diseases.[35,36] The specific affinity of pullulan to ASGP-R could be an valuable pathway in targeted therapy of liver tumors, as it has been reported that pullulan−drug conjugates could enhance the targeting ability to hepatocytes.[31,32] Meanwhile, our previous studies revealed that pH-sensitive pullulan−DOX conjugates (Pu-DOX) nanoparticles were selectively internalized by hepatocarcinoma cells and quickly released drugs inside the acidic endosome/lysosome by the in vitro study.[37]

In this work, four kinds of pH-sensitive Pu-DOX nanoparticles were investigated for delivery of DOX into nuclei hepatic carcinoma cells in nude mice subcutaneous tumor model. These Pu-DOX nanoparticles rapidly released DOX in the acidic environment at pH = 5 while staying relatively stable at neural condition, helping to overcome the intracellular barriers in the way of drug to the cell nuclei.[38] We inspected the multiaspect influence of Pu-DOXs molecular architecture on the nanoparticles characteristics to obtain the optimized nanoparticle. The cellular uptake, intracellular biodistribution, nuclei localization of DOX, and cytotoxicity of the Pu-DOX nanoparticles were evaluated in in vitro cell coculture experiments. In in vivo nude mice subcutaneous hepatic carcinoma model, the accumulation and biodistribution of DOX were observed. Furthermore, the solid tumor volume, the lifetime as well as body weight change of experiment animal were also investigated.

## 2. MATERIALS AND METHODS

**2.1. Materials.** Pullulan (MW 0.2 MDa) was purchased from Hayashibara Biochemical Laboratory (Okayama, Japan). Sodium chloroacetate, isopropyl alcohol, 4′,6-diamidino-2-phenylindole (DAPI), hydrazine hydrate (Hy), oxalic dihydrazide (ODH), succinic dihydrazide (SDH), adipodihydrazide (ADH), and 1-ethyl-3-[3-(dimethylamino) propyl] carbodiimide hydrochloride (EDC·HCl) were purchased from Sigma-Aldrich Co. (St. Louis., MO, USA). Doxorubicin hydrochloride (DOX·HCl, >99%) was obtained from Beijing Zhongshuo Pharmaceutical Technology Development Co. (Beijing, China). All other chemicals are the analytic grade and used as-received. Deionized water (Milli-Q) was used as solvent throughout all experiments.

Human hepatocellular carcinoma cells (HepG2), mouse fibroblast cells (L929), and human cervical carcinoma cells (HeLa) were obtained from Shanghai Institutes for Biological Sciences (Shanghai, China). BALB/c nude mice (4−6 weeks old, 20−25 g) were provided by the Laboratory Animal Center, Sichuan University, China. All handling of animals was performed with the approval of the Institutional Authority for Laboratory Animal Care, Sichuan University.

**2.2. Synthesis and Characterization of pH-Sensitive Pu-DOX Conjugates.** Carboxymethylpullulan (CMP) was prepared as described in previous literature.[37] Subsequently, CMP and four kinds of hydrazine compounds (Hy, ODH, SDH, and ADH) were dissolved in deionized water, then EDC·HCl was added to the solution and stirred at room temperature for 2 h [(COOH):(EDC·HCl):(hydrazine) = 1:1.2:30]. The mixture was dialyzed and freeze-dried to obtain amidated pullulan. Finally, the Pu-DOX conjugate was synthesized as follow: the determined amount of DOX·HCl was added to the amidated pullulan solution and reacted at room temperature for 16 h in dark. The reaction solution was precipitated with ethanol, and then, the Pu-DOX conjugate was obtained by washing the precipitate with ethanol to remove unreacted free DOX·HCl and dried in vacuo for 48 h.

The chemical structure of CMP, amidated pullulans, and Pu-DOXs were confirmed using FT-IR (PerkinElmer FT-IR spectrometer Frontier) and $^1$H NMR (Varian UNITY INOVA 400). The graft degree (DS) of hydrazine compounds on pullulan was measured by oxidation−reduction titration according to the standard method described in Chinese pharmacopoeia.[39] Briefly, a determined amount of HCl was added in the amidated pullulan solution. Then, potassium bromate was used as a volumetric solution, and methyl orange was used as an indicator. The process was carried out under acidic condition. The amount of incorporated DOX was measured by UV absorbance at 485 nm, after the Pu-DOX conjugates were treated with acidic DMSO for 2 h. The drug loading capacity (DLC) and drug encapsulation efficiency (DEE) were calculated by the following equations.

DLC (wt %) = [weight of loaded drug/weight of drug loaded nanoparticles] × 100%

DEE (%) = [weight of loaded drug/weight of drug in feed] × 100%

**2.3. Preparation and Characterization of Pu-DOX Nanoparticles.** The Pu-DOX nanoparticles were obtained by simply resuspending Pu-DOX conjugates in PBS (pH = 7.4). The diameter and size distribution of the obtained nanoparticles were evaluated by dynamic light scattering (DLS, Malvern Nano-ZS, UK) at sample concentration 1.0 mg/mL. For observing the morphology of nanoparticles, the transmission electron microscope (TEM, H-600, Hitachi, Japan) operated at an acceleration voltage of 100 kV was employed.

**2.4. In Vitro Drug Release Profile of Pu-DOX Nanoparticles.** The Pu-DOX nanoparticles (0.3 mg) were dissolved in 1 mL phosphate buffered saline solution (PBS) and were placed in dialysis bags (MWCO 8000−12 000). The dialysis bags were then immersed in 25 mL of PBS with different pH values (pH 5.0 and pH 7.4) and kept in a horizontal shaker maintained at 37 °C for 120 rpm. A 1 mL portion of the medium was removed at different time for a specified interval, and the same volume of fresh PBS was replenished. The released DOX was measured by a fluorescence detector. For monitoring the size change of Pu-DOX nanoparticles, 1 mg of Pu-DOX nanoparticles were dissolved in 1 mL of PBS (pH 7.4 and pH 5.0) and monitored by DLS measurement at certain time intervals.

**2.5. Cell Culture.** HepG2 cells (human liver cancer cells), L929 cells (mouse fibroblast cells), and HeLa cells (human cervical carcinoma cells) were cultured in Dulbecco's Modified Eagle's Medium (DMEM) supplemented with 10% fetal bovine serum, 100 IU/mL penicillin, and 100 μg/mL streptomycin at 37 °C in a humidified atmosphere with 5% $CO_2$.

**2.6. In Vitro Cellular Growth Inhibition, Cellular Uptake of Pu-DOX Nanoparticles and Intracellular Distribution of DOX.** The cytotoxicity of Pu-DOX nanoparticles and free DOX·HCl (for comparing) was measured by the standard methylthiazoltetrazolium


DOI: 10.1021/acsami.5b03150
ACS Appl. Mater. Interfaces 2015, 7, 15855−15865

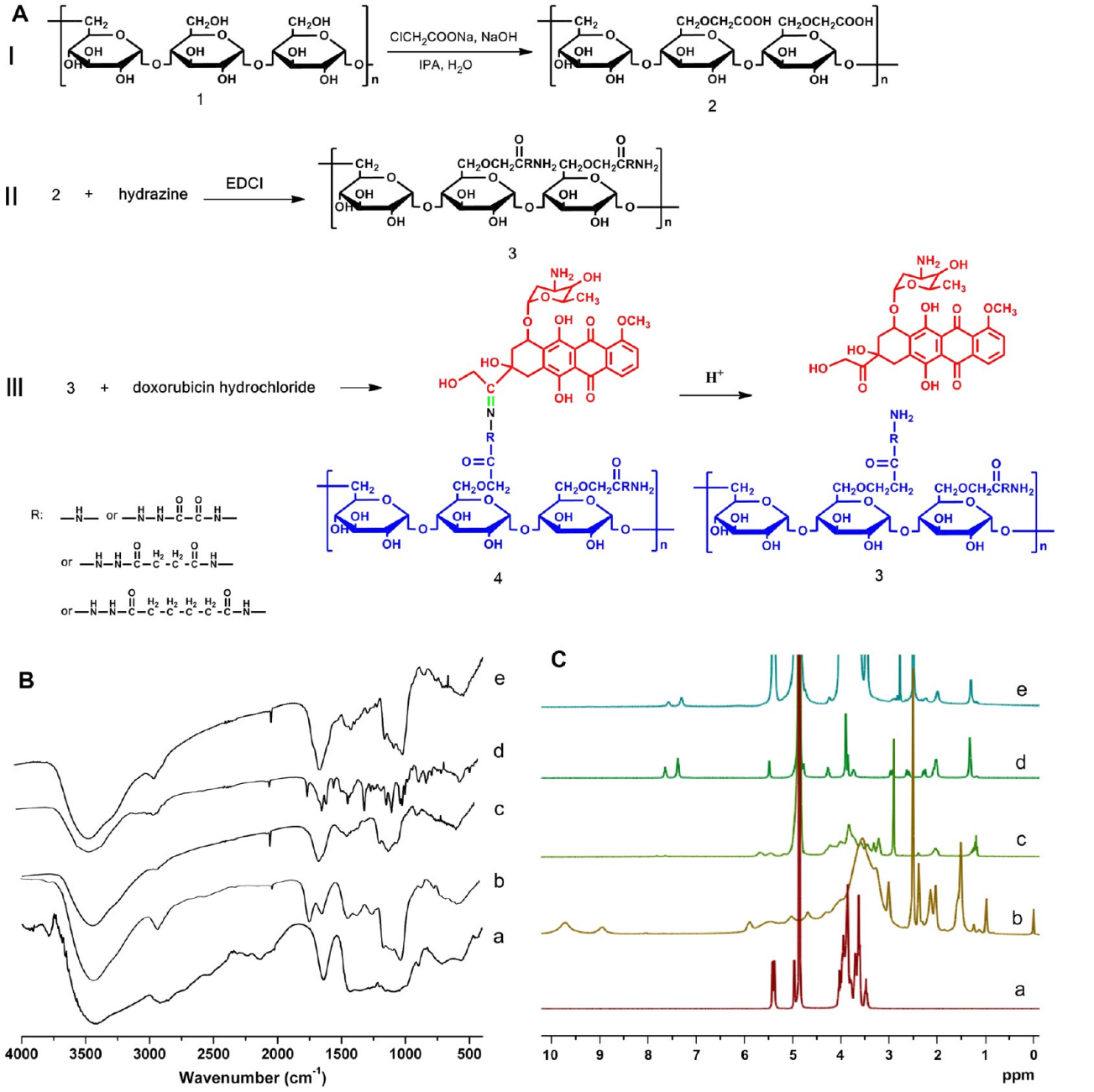


**Figure 1.** Synthesis route of Pu-DOX nanoparticles (A) and representative FT-IR (B) and $^1$H-NMR (C) spectra of (a) pullulan; (b) carboxymethyl pullulan; (c) pullulan−succinic dihydrazide material; (d) DOX·HCl; (e) Pu-SDH-DOX.

(MTT) assay as described previously. [44] HeLa, L929, and HepG2 cells were cultured in 96-well plates at a density of $4 \times 10^3$ cells/well overnight to allow the cells to adhere onto the culture plate surface. Then, 100 $\mu$L of the culture media, in which the equivalent DOX concentrations were 0.01, 0.1, 1.0, 5.0, 10.0, and 50.0 mg/L, respectively, were used to substitute the media in each well. Cells were subsequently incubated for 1 day and then evaluated by MTT assay. Untreated control cells were regarded as 100% viable and all values were expressed as a percentage of the control.

For studying the cellular uptake of Pu-DOX nanoparticles and intracellular distribution of DOX, HeLa, HepG2 and L929 cells at logarithm phase were seeded in 24 well cell culture plates at a cell density of $2 \times 10^4$ cells/well, respectively. After incubated for 24 h, Pu-DOX nanoparticles or DOX·HCl dissolved in PBS at 5 mg/L was added to replace the media in each well. After further incubated for 1.5, 4, and 6 h, the media were removed and these wells were rinsed with PBS (pH = 7.4). The cell nuclei were then stained with DAPI and were observed using confocal laser scanning microscopy (CLSM, Leica TCP SP5, Germany). DOX was excited at 485 nm with the emission at 595 nm.

For the flow cytometry tests, HepG2 cells were seeded in 6-well plate at a density of $3 \times 10^5$ cells/well and incubated for 24 h. The cells were treated with DOX·HCl (1 mg/L) and Pu-DOX nanoparticles (1 mg/L equivalent DOX concentration) for 0.5, 1, 2, and 4 h, respectively. After eliminating culture media and washing the cells with PBS for three times, the cells were harvested by trypsinization and centrifugation (1000 rpm, 5 min). The cells were resuspended in PBS and measured by flow cytometry with excitation and emission wavelengths of 532 and 595 nm, respectively.

**2.7. In Vivo and ex Vivo Biodistribution.** Here, $4 \times 10^6$ cells were injected subcutaneously into the back of BALB/c nude mice (4−6 weeks old, 20−25 g). When the tumor volume reached approximately 150 mm$^3$, Pu-DOX nanoparticles, DOX·HCl, and PBS were injected via tail vein at a dosage of 10 mg DOX/kg


DOI: 10.1021/acsami.5b03150
ACS Appl. Mater. Interfaces 2015, 7, 15855−15865

**Table 1. Preparation of Pu-DOX Conjugate Nanoparticles**

| | feed ratio[a] | 50/10 | 50/20 | 50/30 | 50/40 | 50/50 |
|---|---|---|---|---|---|---|
| Pu-Hy | DLC (%) | 13.59 | 21.20 | 28.49 | | |
| | *d* (nm)[b] | 47.6 | 81.3 | 95.8 | | |
| | PDI | 0.104 | 0.132 | 0.174 | | |
| Pu-ODH | DLC (%) | 14.58 | 23.54 | 34.39 | | |
| | *d* (nm) | 53.0 | 94.4 | 119.6 | | |
| | PDI | 0.089 | 0.187 | 0.073 | | |
| Pu-SDH | DLC (%) | | 29.29 | 35.78 | 39.19 | 41.76 |
| | *d* (nm) | | 118.6 | 128.0 | 135.0 | 148.7 |
| | PDI | | 0.079 | 0.183 | 0.106 | 0.141 |
| Pu-ADH | DLC (%) | | 32.77 | 37.69 | 40.78 | 47.67 |
| | *d* (nm) | | 132.5 | 141.8 | 149.0 | 167.9 |
| | PDI | | 0.147 | 0.059 | 0.154 | 0.124 |

[a]Feed ratio, polymer/DOX·HCl (w/w). [b]Diameter of nanoparticles determined by DLS.

bodyweight. At selected time points, the mice were anesthetized and imaged by an in vivo imaging system (Maestro Ex Pro, CRI, USA) with a 12-bit CCD camera equipped with a near-infrared emission filter (500−950 nm). Mice were sacrificed at 2, 4, and 6 h after injection for comparing ex vivo organ biodistributions of DOX. The excised organs (livers, spleens, kidneys, hearts, lungs, and tumors) were detected using the imaging system. After each imaging point, tumor was frozen rapidly in dry ice, executing 10 $\mu$m thick cryosections. The tissue sections were fixed in cold acetone for 10 min, stained with the DAPI, and captured using CLSM.

In order to quantitatively evaluate the accumulation of DOX in solid tumor, Pu-DOX nanoparticle solutions were injected via the vein at 5 mg DOX/kg bodyweight dose. With 2, 4, 6, and 8 h after the injection, the mice were euthanized, and tumor tissues were collected and weighted. A 0.1 g portion of the tissues was diluted with 1 mL hydrochloride acid (2.0 M) and treated in a tissue grinder (DY89-II, Ningbo XinZhi Biotech, Inc., China). The obtained suspension was then centrifuged at 10 000 rpm for 10 min, and the supernatant was treated with chloroform/isopropanol (3:1 v/v) to extract the doxorubicin. The organic phase was separated and then evaporated. Subsequently, 0.1 mL of DMSO was added to dissolve the doxorubicin and the amount of doxorubicin was measured using UV absorbance at 485 nm.

**2.8. In Vivo Antitumor Effect of Pu-DOX Nanoparticles in Hepatocellular Carcinoma Subcutaneous Model.** Next, $4 \times 10^6$ HepG2 cells were injected subcutaneously into the backs of BALB/c nude mice (4−6 weeks old, 20−25 g). When the tumor volume reached approximately 70−100 $mm^3$, the mice were randomly divided into eight groups and treated by Pu-DOX nanoparticles or DOX·HCl, respectively. Each formulation was injected via the tail vein at a dose of 5 mg/kg (DOX/bodyweight) at a 3 day interval. Each mouse was injected five times during the experiment. Pu-DOX nanoparticles were also administered at higher dose (20 mg/kg) to determine if the antitumor effect could be enhanced. The tumor volume and body weight were recorded at prescribed time intervals. The tumor volume was calculated as follows:

Tumor volume ($mm^3$) = width$^2$ × length/2.

After 25 days, 3 mice were sacrificed; the liver, heart, spleen, lung, and kidney were separated, washed with PBS, and fixed in 10% formaldehyde for histological examination. Other animals were euthanized when the implanted tumor volume reached 1000 $mm^3$, which was considered as the end point of survival data. The same method was used for further investigating the systemic toxicity of Pu-DOX nanoparticles to normal nude mouse.

**2.9. Statistical Analysis.** The results are presented as the mean value with standard deviation (mean ± SD). Statistical analysis was performed using two-tailed, unpaired *t* tests between data sets. Probability values less than 0.05 ($p < 0.05$) were considered to indicate a statistically significant result.

## 3. RESULTS AND DISCUSSION

**3.1. Synthesis and Characterization of Pu-DOX Conjugates.** A series of Pu-DOX conjugates were successfully synthesized via three synthesis steps, including carboxymethylation, amidation, and condensation reaction according to the synthesis route presented in Figure 1A. Carboxymethylpullulan was first synthesized as described in previous literature.[37] Then, four kinds of hydrazine compounds (Hy, ODH, SDH, and ADH) were reacted with carboxymethylpullulan, respectively. To ensure complete reaction, carboxymethyl pullulan with graft degree 65.1% was reacted with excessive hydrazine (30/1 molar ratio of hydrazine/carboxylic group). The graft degrees of hydrazine compounds (Hy, ODH, SDH, ADH) on carboxymethylpullulan were 98.96%, 96.31, 95.19%, and 82.04%, respectively. The formation efficiency of amide bond decreased along with increasing length of the hydrazine compounds. The possible reason for this was that the reaction activity and the opportunity to contact between hydrazine/carboxylic groups reduced with increasing molecular chain length.

DOX was bonded to pullulan through the formation of a pH-sensitive hydrazone bond. In this way, four series of Pu-DOX conjugates were synthesized by changing the feeding amount of DOX (Table 1). FT-IR and $^1$H NMR spectra of representative carboxymethylpullulan, amidated pullulan, and conjugates were shown in Figure 1B and C. The FT-IR spectrum of carboxymethylpullulan exhibited the characteristic absorption band at 1736 $cm^{-1}$ due to the C═O stretching vibration of the carboxylic groups. After succinic dihydrazide was grafted onto pullulan chain, carboxylic groups C═O stretching peak at 1736 $cm^{-1}$ of pullulan-succinic dihydrazide disappeared, which indicated the formation of amide bond. Meanwhile, the Pu-DOX conjugate showed a strong peaks about 1008 $cm^{-1}$, which was attributed to the stretching of conjugated DOX by comparing with the spectrum of DOX·HCl. The $^1$H NMR signals of carboxymethylpullulan at 8.7−10.0 ppm were contraposed to carboxylic group. Compared with the spectrum of pullulan-succinic dihydrazide polymer and DOX·HCl, new resonances appeared at 7.5−8.0 ppm in $^1$H NMR spectrum of Pu-DOX, confirmed that DOX was bounded to pullulan. For each pullulan derivate, the content of DOX in Pu-DOX was controlled by adjusting pullulan derivate/DOX feed ratio in the reaction. With the increase of feeding DOX, the DLC of Pu-DOX conjugates increased accordingly. The DLC of pullulan-adipodihydrazide-DOX conjugate (Pu-ADH-DOX) could go up to 47.67 wt % without precipitation when the feeding ratio of pullulan-adipodihydrazide derivate/DOX reached 50/50.


DOI: 10.1021/acsami.5b03150
ACS Appl. Mater. Interfaces 2015, 7, 15855−15865

The highest DLC without precipitation of Pu-Hy-DOX, Pu-ODH-DOX, and Pu-SDH-DOX were 28.49, 34.39, and 41.76 wt %, at pullulan derivate/DOX 50/30, 50/30, and 50/50, respectively. Further increasing the DOX amount resulted in the formation of red muddy precipitation. On the other hand, with the same feed ratio 50/30, the DLC increased obviously along with the length of spacer from 28.49 wt % to 37.69 wt %. The possible reason was that the increased chain spacer was beneficial to improve the flexibility of DOX molecule, so that improving the internal space utilization, and increasing the DLC. Therefore, the DLC could be adjusted by both the spacer and the feed ratio in the conjugate reaction.

According to the above results, for intensively investigating the influence of polymer structure on the nanoparticular carriers, four kinds of Pu-DOXs with similar DLC (about 18 wt %) were synthesized by adjusting the feed ratio of pullulan derivate to DOX (Table 2) and were used in the subsequent investigation.

**Table 2. Pu-DOX Conjugate Nanoparticles with DLC 18 w/w %**

| samples | Pu-Hy-DOX | Pu-ODH-DOX | Pu-SDH-DOX | Pu-ADH-DOX |
|---|---|---|---|---|
| feed ratio[a] | 50/19 | 50/17 | 50/16 | 50/15 |
| DLC (%) | 18.73 | 18.57 | 18.97 | 18.28 |
| $d$ (nm)[b] | 73.5(0.197) | 79.8(0.089) | 92(0.034) | 107.6(0.027) |

[a]Feed ratio, polymer/DOX·HCl (w/w). [b]Diameter of nanoparticles determined by DLS. The numbers in the brackets represent the PDI.

**3.2. Characterization and pH Triggered Drug Release of Pu-DOX Nanoparticles.** All the synthesized Pu-DOX could easily self-aggregate to form nanoparticles with core–shell structure by simply resuspending the Pu-DOX in aqueous medium. Figure 2A and B showed the typical TEM image and DLS graph of Pu-ADH-DOX nanoparticle. The TEM image (Figure 2A) clearly revealed that the nanoparticles were dispersed as individual particles with a well-defined spherical shape in aqueous solution. This would lay the favorable foundation for the nanoparticles to accumulate in tumor site through EPR effect. Figure 2B showed narrow size distribution of nanoparticle, in keeping with the observation in TEM image. The average hydrodynamic diameter of the nanoparticles prepared in this work was ranged from 50 to 170 nm (Table 1). Increasing the feed amount of DOX during the synthesis process directly led to increase of drug content in the Pu-DOX, closely related with particle size. The particle size with same drug loading content increased along with chain length of spacers (Table 2), probably because the increased length of chain extended the internal space of hydrophobic core, and resulted in the nanoparticles diameter enlarge.

Drug release behavior of the above-mentioned four nanoparticles were determined by dialysis method in PBS at pH 7.4 and pH 5.0 (corresponding to the pH value of endosome), respectively. The results (Figure 2C) showed that more than 90% of loaded DOX released from Pu-DOX nanoparticles within several hours at pH 5.0 since the breakage of hydrazone linkers accelerated the release of drug at lower pH values. On the other hand, only less than 15% of DOX could release at pH 7.4 even after 12 h incubation. The release profile in vitro indicated that the nanoparticles could keep stabile during

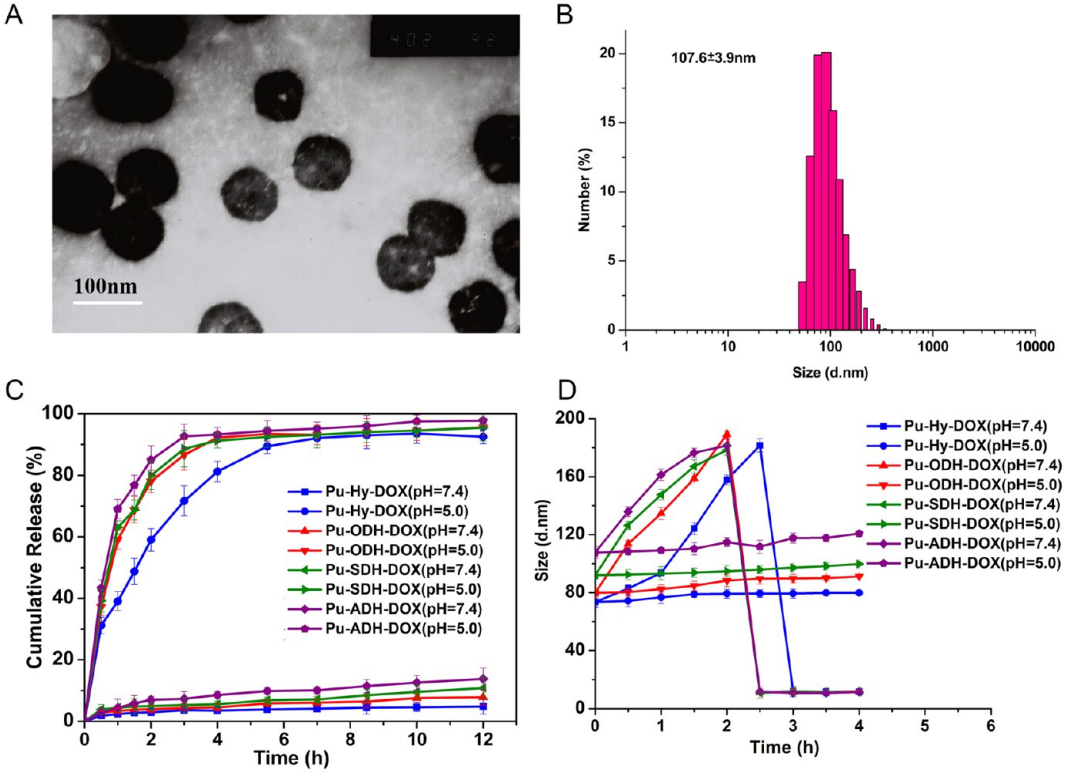


**Figure 2.** TEM (A) and DLS (B) image of Pu-ADH-DOX nanoparticles (DLC 18 wt %). (C) In vitro drug release behavior of Pu-Hy-DOX, Pu-ODH-DOX, Pu-SDH-DOX, and Pu-ADH-DOX nanoparticles (DLC 18 wt %) at different pH values ($n$ = 3). (D) Size change of Pu-Hy-DOX, Pu-ODH-DOX, Pu-SDH-DOX, and Pu-ADH-DOX nanoparticles (DLC 18 wt %) during the drug release process ($n$ = 3).


DOI: 10.1021/acsami.5b03150
ACS Appl. Mater. Interfaces 2015, 7, 15855–15865

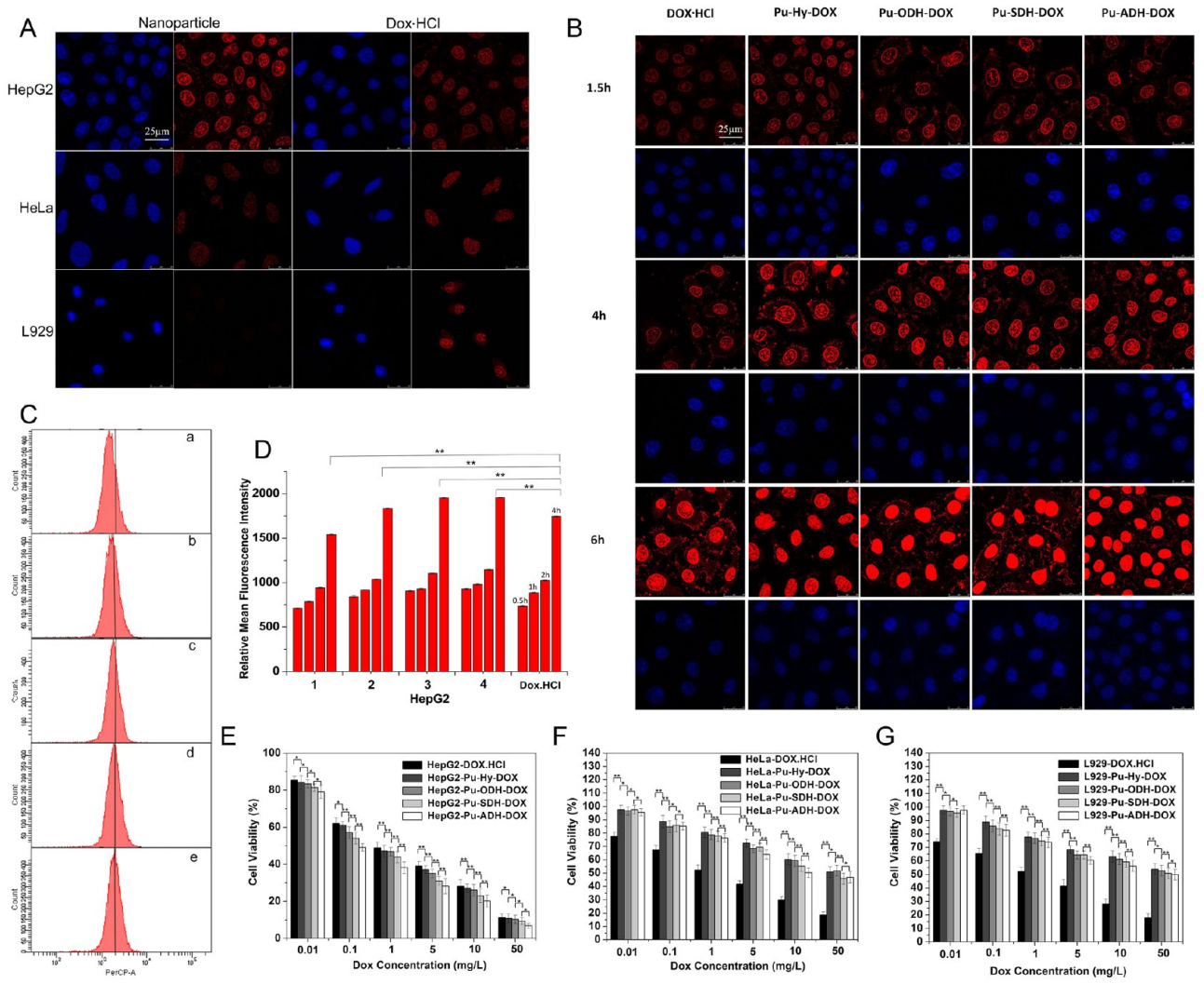


**Figure 3.** (A) CLSM images of HepG2, HeLa, and L929 cell lines incubated with Pu-Hy-DOX nanoparticles and DOX·HCl for 1.5 h (DOX concentration 5 mg/L). (B) CLSM images of HepG2 cells incubated with four kinds of Pu-DOX nanoparticles (Pu-Hy-DOX, Pu-ODH-DOX, Pu-SDH-DOX and Pu-ADH-DOX) and DOX·HCl for 1.5, 4, and 6 h (DOX concentration 5 mg/L). (C) Flow cytometry of HepG2 cells incubated with Pu-DOX nanoparticles: (b) Pu-Hy-DOX, (c) Pu-ODH-DOX, (d) Pu-SDH-DOX, (e) Pu-ADH-DOX, and DOX·HCl (a) for 4 h (DOX concentration 1 mg/L). (D) Quantitative analysis DOX uptake by HepG2 cells via flow cytometry incubated with four kinds of Pu-DOX nanoparticles and DOX·HCl for 0.5, 1, 2, 4 h (DOX concentration 1 mg/L). The cytotoxicity of four kinds of Pu-DOX nanoparticles and DOX·HCl against HepG2 (E), HeLa (F), and L929 cells (G) at various DOX concentrations, respectively. DLC of all nanoparticles were about 18 wt % (see Table 2). Data were presented as mean ± SD, * $p < 0.05$. The scale bar = 25 $\mu$m.

circulation and could rapidly release the loaded DOX in the acidic endosomes/lysosomes where the pH range is 4.0−6.0. As shown in Figure 2C, the drug release rate was also related with the alkane chain length of spacers. For Pu-Hy-DOX conjugate, it took about 7 h to reach the almost complete (90%) release. In comparison, Pu-ADH-DOX nanoparticles with the longest spacer reached 90% release in about 3 h; Pu-SDH-DOX and Pu-ODH-DOX released 90% of loaded drug in about 4 h. The reason might be that nanoparticle with shorter spacer, such as Pu-Hy-DOX nanoparticle, had more compact internal core structure and smaller size, which postponed the nanoparticle degradation speed in the low pH value solution. Meanwhile, under the condition of pH 7.4, the sizes of nanoparticles kept their initial size within the releasing process (Figure 2D). When the pH value decreased to 5.0, the sizes of all the nanoparticles rapidly increased in the first 2 h. This phenomenon, in combination with the previous drug release results, indicated that hydrophobic DOX was detached from the Pu-DOX nanoparticles under acidic condition due to the cleavage of pH-sensitive hydrazone, which resulted in the subsequent loose structure of nanoparticles because of the decreased hydrophobic interaction in the core. After 2−2.5 h, no nanoparticles could be detected, implying that there were no longer enough hydrophobic DOX in the Pu-DOX conjugates to keep the stable core−shell structure and the nanoparticles completely disassembled. This result was in accordance with the drug release data; the size change of Pu-Hy-DOX nanoparticle with the shortest spacer was slower than that of other Pu-DOX nanoparticles.

**3.3. Cellular Uptake, Intracellular Distribution, and Growth Inhibition Effect of Pu-DOX Nanoparticles.** Pu-DOX nanoparticles were selectively internalized by hepatocytes because of the specific affinity of pullulan to ASGP-R, which highly expressed on hepatocyte membrane. Figure 3A illustrated the CLSM observation on cellular uptakes of Pu-Hy-DOX nanoparticles by HepG2, HeLa, and L929 cells after


DOI: 10.1021/acsami.5b03150
ACS Appl. Mater. Interfaces 2015, 7, 15855−15865

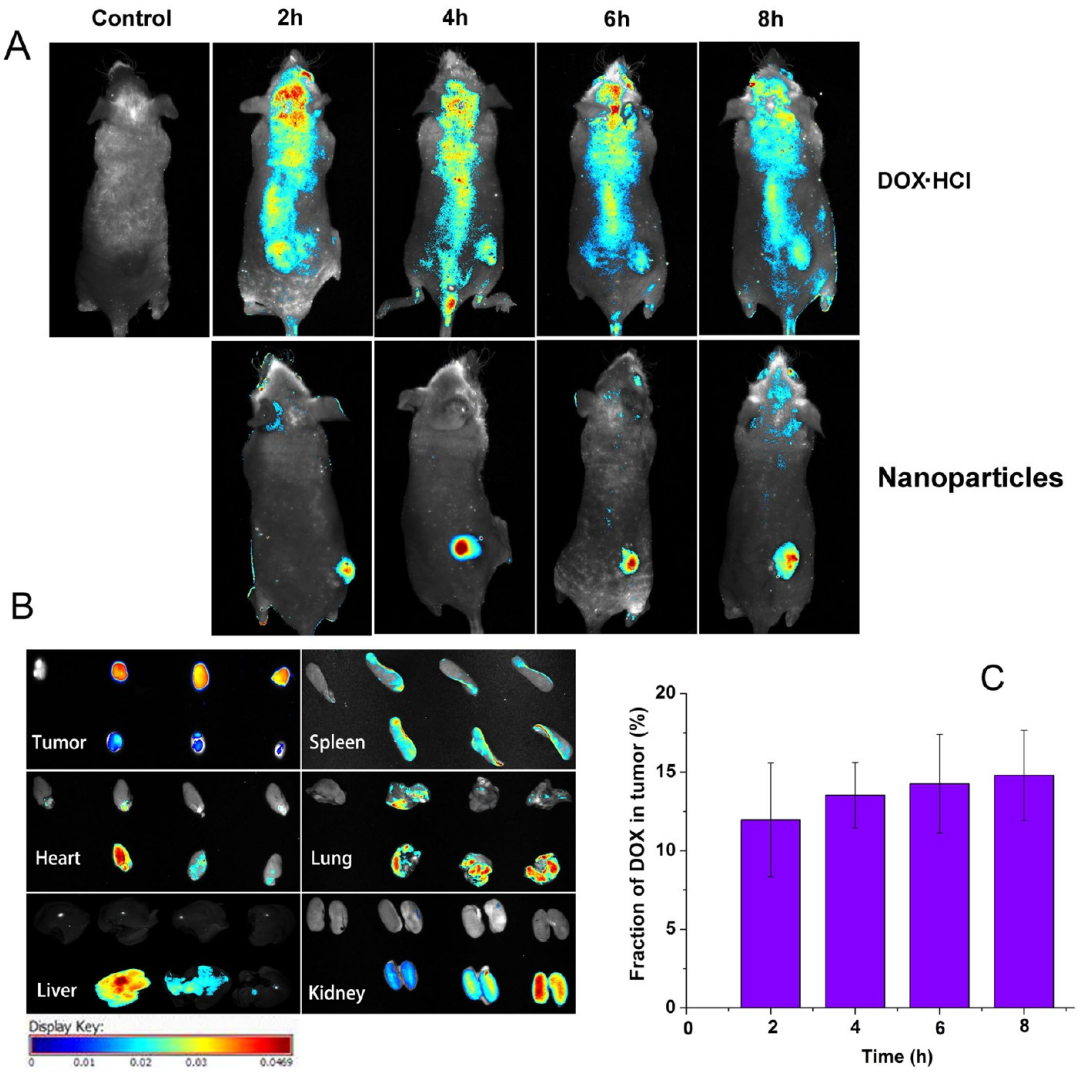


**Figure 4.** (A) In vivo optical fluorescence images of hepatoma tumor-bearing nude mice administrated with Pu-ADH-DOX nanoparticle and DOX·HCl at 2, 4, 6, and 8 h postinjection (10 mg DOX/kg bodyweight). (B) Optical fluorescence images of different organs (tumors, spleens, hearts, lungs, livers, and kidneys) at 2, 4, and 6 h postinjection (10 mg DOX/kg bodyweight) of Pu-ADH-DOX nanoparticles and DOX·HCl. (C) Drug fraction in tumor tissue of the total injected DOX at 2, 4, 6, and 8 h postinjection of Pu-ADH-DOX nanoparticles (5 mg DOX/kg bodyweight). DLC of all nanoparticles were about 18 wt % (see Table 2). Data were presented as mean ± SD, * $p < 0.05$.

incubated for 1.5 h. When DOX·HCl was used, there were no significant differences among the three cell lines in fluorescence intensity of internalized DOX. On the other hand, when Pu-DOX nanoparticles was used, red fluorescence of DOX in HepG2 cells became obviously stronger than thatof DOX·HCl, but in HeLa and L929 cells, much weaker fluorescence signals were observed compared with that of DOX·HCl. In our previous work,[37] the results of competitive cellular uptake of pullulan micelles and pure pullulan revealed that pullulan micelles binding to ASGPR on HepG2 membrane competitively with pure pullulan. Therefore, it could be presumed that pullulan in the nanoparticle shell retained it binding activity and specificity, and served as the ligand to bind the ASGP-R to promote cellular uptake of hepatocarcinoma cells via receptor-mediated endocytosis.

It was worthwhile to notice that red fluorescence of DOX was observed in the cell nuclei. Since the action mechanism of DOX is to intercalate DNA and RNA in the nuclei, the enhanced nuclei localization of DOX by Pu-DOX nanoparticles is particularly crucial for enhancing the antitumor efficacy of nanoparticular formula. Free DOX·HCl diffuses into nuclei because of its high affinity with nucleic acids, but normal nanoparticles that are internalized through endocytosis pathway generally entrap the DOX in endosome/lysosome. The observation in CLSM indicated that, in agreement with the in vitro drug release behavior in acidic PBS (pH = 5.0), the pH-sensitive Pu-DOX nanoparticles could rapidly release DOX in the acidic environment of endosome/lysosome. As a result, the released free DOX diffused into nuclei in a short time as observed in CLSM.

Improved internalization of Pu-DOX nanoparticles into HepG2 cells were observed for nanoparticles with longer alkane chain, as shown in Figure 3B for 1.5, 4, and 6 h coincubation of HepG2 cells with these four nanoparticles. The quantitative monitoring was also conducted using flow cytometry. Figure 3C showed the representative flow cytometric graphs of HepG2 cells after 4 h coincubation with four kinds of nanoparticles. The quantitative results of flow cytometry indicated that after different coincubation time from 0.5 to 4 h, the cellular DOX level of Pu-ODH-DOX, Pu-SDH-


DOI: 10.1021/acsami.5b03150
ACS Appl. Mater. Interfaces 2015, 7, 15855−15865

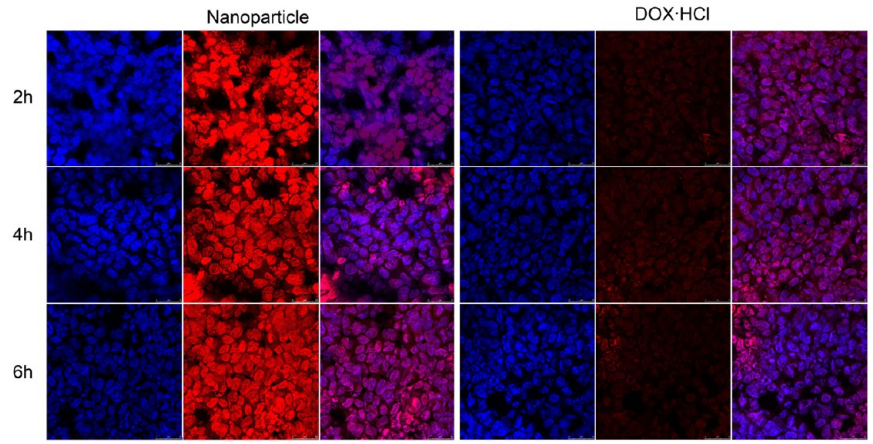


**Figure 5.** CLSM images of tumor cryosections at 2, 4, and 6 h postinjection of Pu-ADH-DOX nanoparticles and DOX·HCl. Blue fluorescence shows nuclear staining with DAPI, and red fluorescence shows the location of DOX. DLC of nanoparticle was about 18 wt % (see Table 2). The scale bar = 25 $\mu$m.

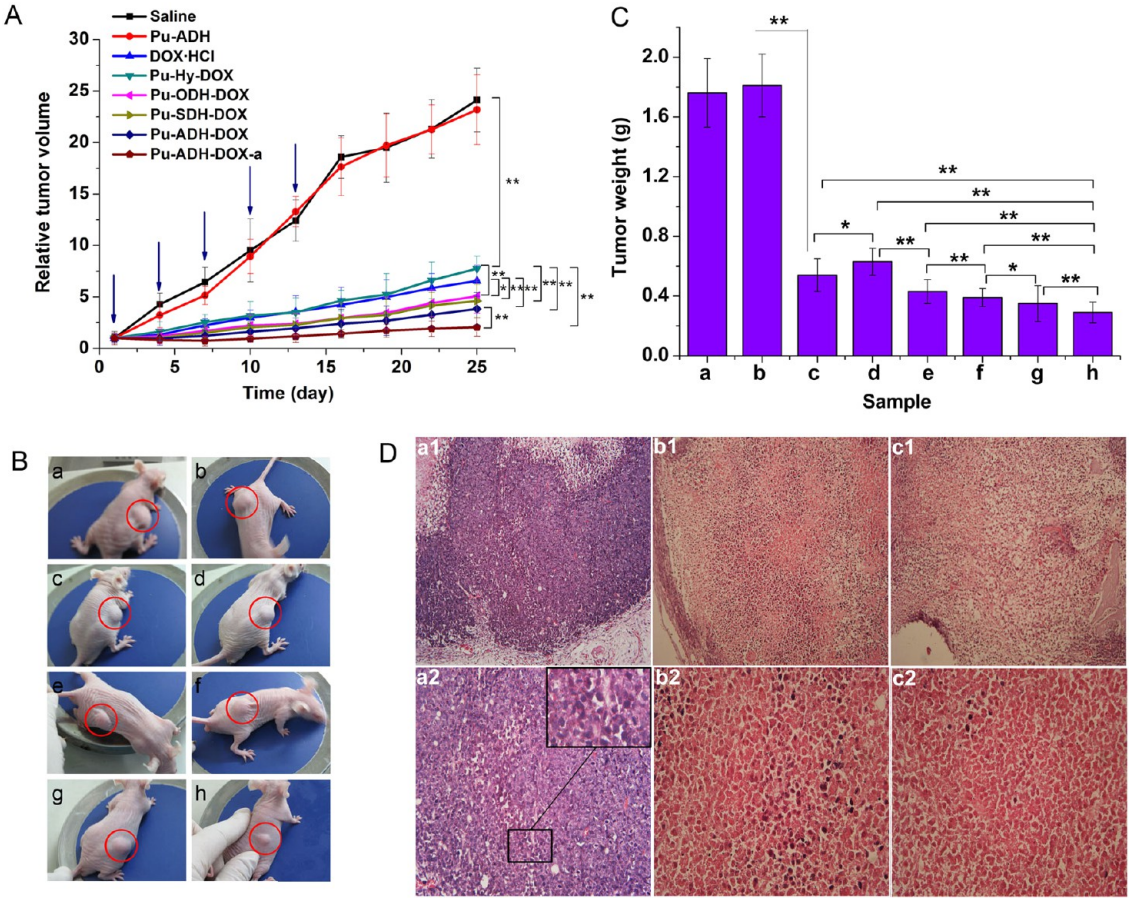


**Figure 6.** (A) Tumor volume change in the hepatoma tumor-bearing nude mice after injection of saline and various DOX formula ($n$ = 6). (B) Visual observation and (C) tumor weight of hepatoma tumor-bearing nude mice after injection of saline and various DOX formulas for 25 days: (a) saline; (b) Pu-ADH; (c) DOX·HCl; (d) Pu-Hy-DOX; (e) Pu-ODH-DOX; (f) Pu-SDH-DOX; (g) Pu-ADH-DOX; (h) Pu-ADH-DOX-a. DOX dosage of c−g was 5 mg/kg bodyweight; that of h was 20 mg/kg bodyweight. (D) Histological observation for tumor treated with (a) saline; (b) DOX·HCl; (c) Pu-ADH-DOX (DOX dosage 5 mg/kg bodyweight; a1, b1, c1: ×40; a2, b2, c2: ×200). Data were presented as mean ± SD, * $p$ < 0.05.

DOX, and Pu-ADH-DOX nanoparticles was higher than that of DOX·HCl, but Pu-Hy-DOX nanoparticles delivered less DOX into HepG2 cells than DOX·HCl (Figure 3D).

As a well-known cytotoxic drug, DOX·HCl showed a similar growth-inhibitory effect against HepG2, HeLa, and L929 cells (Figure 3E, F, and G). In contrast, Pu-DOX nanoparticles expressed different cytotoxicity against different cell lines. In coculture with the HepG2 cell, the nanoparticles showed stronger tumor cell growth inhibition ability than that of DOX·HCl, and the Pu-ADH-DOX nanoparticle with longer alkane


DOI: 10.1021/acsami.5b03150
ACS Appl. Mater. Interfaces 2015, 7, 15855−15865

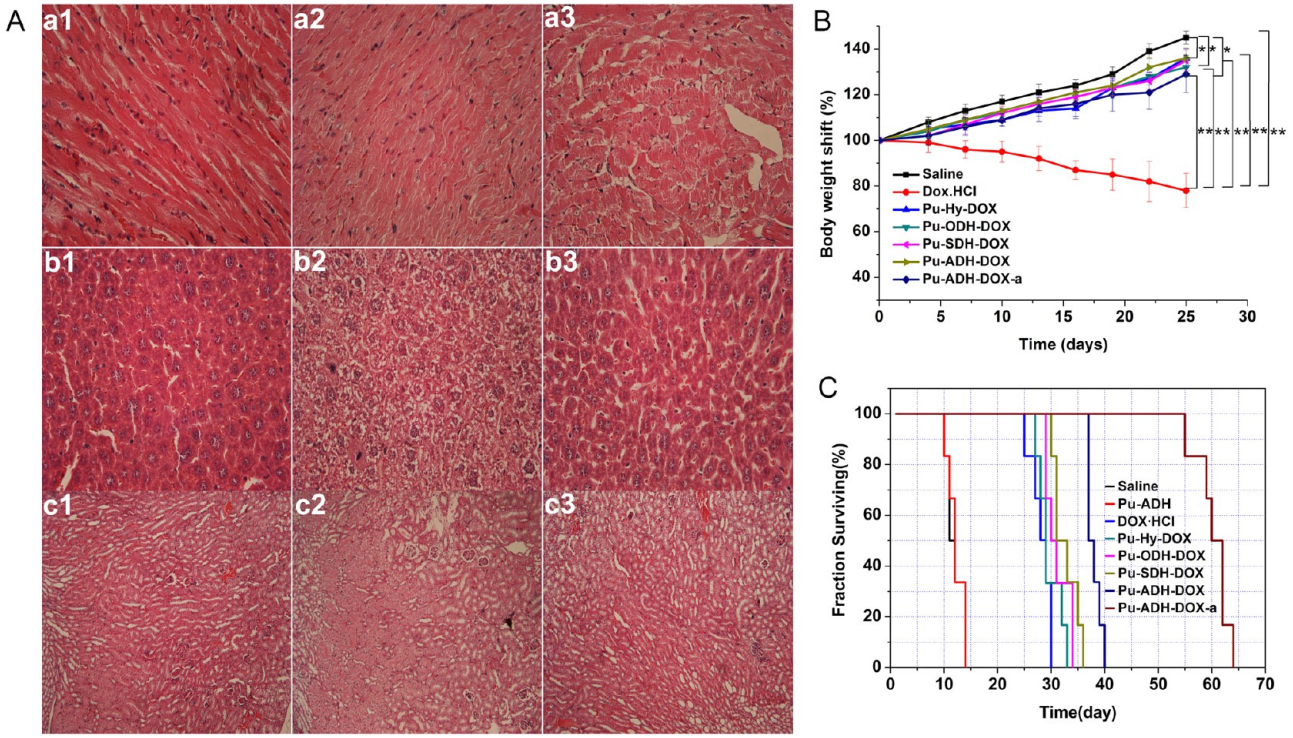


**Figure 7.** (A) Histological observation of heart (a), liver (b), and kidney (c) from tumor-bearing nude mice administrated with saline (a1, b1, c1), DOX·HCl (a2, b2, c2), and Pu-ADH-DOX nanoparticle (a3, b3, c3) (×200). (B) Bodyweight change and (C) survival rates of hepatoma tumor-bearing nude mice after injection of saline and various DOX formulas ($n = 6$). DOX dosage was 5 mg/kg bodyweight except that for Pu-ADH-DOX-a which was 20 mg/kg bodyweight. Data were presented as mean ± SD, * $p < 0.05$.

chain spacers had the strongest antitumor ability. But for HeLa and L929 cells, cytotoxicity of Pu-DOX nanoparticles was significantly less than that of DOX·HCl. These MTT test results were in accordance with those found in Figure 3A, where the cellular uptake of nanoparticles by HepG2 cells was higher than that of DOX·HCl, whereas the cellular uptake of nanoparticles by HeLa and L929 cells was less than that of DOX·HCl. Thus, it was predicted that the enhanced antiproliferation effect on HepG2 cells by Pu-DOX nanoparticles could be ascribed to the enhanced cellular uptake by hepatocarcinoma cells.

**3.4. Tumor Accumulation of Pu-ADH-DOX Nanoparticle.** Free DOX·HCl and Pu-ADH-DOX (10 mg DOX/kg body weight) were injected intravenously into hepatocyte tumor-bearing nude mice, respectively, to investigate the biodistribution of DOX in vivo. When the mice were treated with DOX·HCl, DOX fluorescence was found wildly dispersed in the body with slightly stronger intensity at the tumor site (Figure 4A). On the other hand, when DOX was injected in Pu-ADH-DOX nanoparticlular formula, DOX fluorescence extensively accumulated at tumor site, with almost undetectable distribution in other parts of the body. In addition, the intense fluorescence could last for over 6 h in the tumor site.

Fluorescence of the excised tumor tissue and other organs at 2, 4, and 6 h after injection were imaged (Figure 4B). Similar with the whole-body fluorescence images, DOX fluorescence in tumor treated by nanoparticles was much stronger than that treated by DOX·HCl. Meanwhile, strong signals were detected in heart, lung, spleen, and liver in animal treated by DOX·HCl, but for Pu-ADH-DOX nanoparticle treated animals, the fluorescence in these organs was much weaker. This showed that Pu-ADH-DOX nanoparticles increased the tumor accumulation and decreased untargeting distribution of DOX by way of efficient EPR effect. With pH-sensitive Pu-ADH-DOX nanoparticles, about 12% of injected DOX could accumulate in tumor 2 h postinjection (Figure 4C); this gradually increased to 15% at 8 h.

Frozen sections of excised tumor were stained with DAPI to locate the nuclei (blue fluorescense) and observed with CLSM (Figure 5). Likewise, the images clearly showed that DOX signals of nanoparticle group were remarkablely stronger than that of the free DOX·HCl group. More importantly, the red signal of DOX was found completely overlapped with the nuclei blue signal, and no red fluorescence was found between nuclei. This indicated that in the hepatic carcinoma subcutaneous animal model, DOX was effectively delivered to hepatoma cells and further rapidly diffused into tumor cell nuclei, taking advantage of EPR effect and pH-sensitive release performance of the Pu-ADH-DOX nanoparticle.

**3.5. In Vivo Antitumor Effect of Pu-DOX Nanoparticles.** Nude mice bearing subcutaneous hepatic carcinoma were administrated with free DOX·HCl (5 mg DOX/kg body weight) and four kinds of Pu-DOX nanoparticles (DLC 18 wt %, 5 mg DOX/kg body weight). After 25 days, the relative tumor volume without drug treatment (saline and Pu-ADH groups) reached about 25 (Figure 6A). When DOX·HCl was injected, the relative tumor volume was only one-third of the untreated group, showing the effectiveness of DOX·HCl as an anticanter chemotherapeutic. When the mice were treated with Pu-DOX nanoparticles, tumor growth was also effectively suppressed, but the relative tumor volume in Pu-Hy-DOX treated group was bigger, although not significantly, than that of DOX·HCl treated group. With the increase of alkane chain length in conjugate spacer, the antitumor effect of nanoparticles


DOI: 10.1021/acsami.5b03150
ACS Appl. Mater. Interfaces 2015, 7, 15855−15865

improved. The relative tumor volume of Pu-ODH-DOX, Pu-SDH-DOX, and Pu-ADH-DOX treated groups became significantly smaller than that of DOX·HCl and Pu-Hy-DOX treated groups. After 25 days, the relative tumor volume of Pu-ADH-DOX treated mice was suppressed to one-half of Pu-Hy-DOX treated mice. These results indicated that inclusion of different spacer structure and pH-sensitive characteristics could increase the antitumor efficiency in vivo. Further, at high DOX dose (20 mg DOX/kg body weight), the tumor growth inhibition ability of Pu-ADH-DOX nanoparticle was obviously enhanced compared with the 5 mg group. Visual observation of the nude mice was highly in agreement with these results (Figure 6B).

After 25 days, the tumors of all groups were removed and weighed (Figure 6C). The tumor weights in nanoparticle treated groups were obviously lower than that of control groups (saline and Pu-ADH). However, tumor suppression of Pu-Hy-DOX was slightly inferior to free DOX·HCl, whereas the other three kinds of nanoparticles were significantly superior to free DOX·HCl and Pu-Hy-DOX. Histological observation of the excised tumor clearly revealed the differences in tumor tissues after 25 days postinjection of saline, DOX·HCl, and Pu-ADH-DOX (Figure 6D). For saline treated mice, purple stained nuclei occupied most of the area. Necrosis area and neoplastic cells were hardly observed in most areas (Figure 6Da). But in tumor tissue treated with DOX·HCl, the necrosis area was obvious (Figure 6Db). In Pu-ADH-DOX treated tumor tissue, more serious necrosis and neoplastic cells were found (Figure 6Dc).

These in vivo and ex vivo results demonstrated that enhanced tumor accumulating and nuclei distrubition of DOX were achieved using pH-sensitive Pu-DOX nanoparticles as carriers. Subsequently, tumor growth was suppressed more effectively, compared with DOX·HCl. The high antitumor activity of the Pu-DOX nanoparticles was attributed to higher accumulation in tumor via EPR effect, hepatic targeting by receptor mediated endocytosis, and the accelerated release of DOX from endosomes.

**3.6. Systemic Toxicity of Pu-DOX Nanoparticles in Nude Mice.** DOX·HCl is well-known for its severe side effects dominated by heart toxicity. Compared with normal heart, liver, and kidney tissues (Figure 7Aa1, b1, and c1), in histological observation of heart tissue from DOX·HCl treated mice, puff cardiomyocyte nucleus with vacuole and undense cytoplasm, as well as acute inflammatory cells infiltration, was observed (Figure 7Aa2); in liver tissue, the hepatic cells arranged mussily and the structure of hepatic lobule disappeared (Figure 7Ab2); in kidney tissue, pyknosis of glomerulus, absent lumen, and hydropic degeneration were observed (Figure 7Ac2). In contrast, all the organs from mice treated with Pu-ADH-DOX were mostly normal (Figure 7Aa3, b3, and c3). Obviously, the damages on these organs due to the side effects of DOX·HCl were efficaciously relieved. Meanwhile, the fluctuation in body weight, as a common factor for assessing in vivo toxicity, actually increased up to 35% when treated with the four kinds of Pu-DOX nanoparticles, even when the equivalent DOX dose reached 20 mg/kg for Pu-ADH-DOX nanoparticle (Figure 7B), in contrast to the 22% bodyweight loss in mice treated with DOX·HCl. As the result of the enhanced antitumor efficiency and reduced side effects, the Pu-DOX nanoparticles remarkably elongated the life span of tumor bearing mice (Figure 7C). With the same dose of 5 mg DOX/kg bodyweight, the average survive time of tumor bearing mice prolonged from 28.2 d for DOX·HCl group to 29.7 d for Pu-Hy-DOX group. It was worth noting that the tumor volume of Pu-Hy-DOX group was bigger than that of DOX·HCl group at 25 d post injection. Nevertheless, Pu-Hy-DOX elongated the mice life span more than DOX·HCl, probably because of its lower systemic toxicity. For Pu-ADH-DOX treated group, the average life span of mice elongated to 38.0 d at the same DOX dose of 5 mg DOX/kg bodyweight. Further increasing the dose to 20 mg DOX/kg bodyweight, Pu-ADH-DOX elongated average survive time of mice to 60.3 d. But mice injected with 20 mg DOX/kg bodyweight of DOX·HCl all died within 24 h. Therefore, it is reasonable to consider that Pu-DOX nanoparticles brought out high in vivo efficacy against hepatic carcinoma with decreased toxic side effects.

## 4. CONCLUSION

The pH-sensitive pullulan−doxorubicin conjugate nanoparticles with high drug loading capacity, which were stable in physiological conditions and rapidly released DOX at reduced pH, were investigated for their application to delivery DOX to hepatic carcinoma cells in subcutaneous tumor model. In in vitro cell culture, these nanoparticles were selectively internalized by hepatic carcinoma cells, released DOX in acidic endosome/lysosome condition and transferred the drug into cell nuclei to induce the cancer cell apoptosis. In nude mice bearing hepatic carcinoma, these nanoparticles accumulated in tumor sites through EPR effect. They were internalized by tumor cells and localized the drug in cell nuclei. These Pu-DOX nanoparticles could more effectively inhibit the tendency of rapid tumor growth and elongated animal lifetime than DOX·HCl.

## AUTHOR INFORMATION

### Corresponding Authors

*Mailing address: Room 803, Biomaterials Building, Sichuan University, Chengdu 610064, China. Tel.: +86-28-85417654. Fax: +86-28-85417654. E-mail: sunyong8702@scu.edu.cn (Y.S.).

*Mailing address: Room 706, Biomaterials Building, Sichuan University, Chengdu 610064, China. Tel.: +86-28-85416196. Fax: +86-28-85410246. E-mail: fan_yujiang@scu.edu.cn (Y.F.).

### Funding

This work was sponsored by National Natural Science Foundation of China (grants 21174090 and 51403138).

### Notes

The authors declare no competing financial interest.

## ACKNOWLEDGMENTS

The authors thank Mr. Xiaoli Zhu for his help in animal experiments.

## REFERENCES

(1) Luo, Y. L.; Shiao, Y. S.; Huang, Y. F. Release of Photoactivatable Drugs from Plasmonic Nanoparticles for Targeted Cancer Therapy. *ACS Nano* **2011**, *5*, 7796−7804.

(2) Xiong, X. B.; Lavasanifar, A. Traceable Multifunctional Micellar Nanocarriers for Cancer-Targeted Co-delivery of MDR-1 siRNA and Doxorubicin. *ACS Nano* **2011**, *5*, 5202−5213.

(3) Fornari, F. A.; Randolph, J. K.; Yalowich, J. C.; Ritke, M. K.; Gewirtz, D. A. Interference by Doxorubicin with DNA Unwinding in MCF-7 Breast Tumor Cells. *Mol. Pharmacol.* **1994**, *45*, 649−656.



DOI: 10.1021/acsami.5b03150
*ACS Appl. Mater. Interfaces* 2015, 7, 15855−15865

(4) Momparler, R. L.; Karon, M. S.; Siegel, E.; Avila, F. Effect of Adriamycin on DNA, RNA, and Protein Synthesis in Cell-free Systems and Intact Cells. *Cancer. Res.* **1976**, *36*, 2891−2895.
(5) Du, Y. Z.; Weng, Q.; Yuan, H.; Hu, F. Q. Synthesis and Antitumor Activity of Stearate-g-dextran Micelles for Intracellular Doxorubicin Delivery. *ACS Nano* **2010**, *4*, 6894−6902.
(6) Carvalho, C.; Santos, R. X.; Cardoso, S.; Correia, S.; Oliveira, P. J.; Santos, M. S.; Moreira, P. I. Doxorubicin: The Good, the Bad and the Ugly Effect. *Curr. Med. Chem.* **2009**, *16*, 3267−3285.
(7) Smith, L. A.; Cornelius, V. R.; Plummer, C. J.; Levitt, G.; Verrill, M.; Canney, P.; Jones, A. Cardiotoxicity of Anthracycline Agents for the Treatment of Cancer: Systematic Review and Meta-analysis of Randomised Controlled Trials. *BMC Cancer* **2010**, *10*, 337.
(8) Nukolova, N. V.; Oberoi, H. S.; Cohen, S. M.; Kabanov, A. V.; Bronich, T. K. Folate-decorated Nanogels for Targeted Therapy of Ovarian Cancer. *Biomaterials* **2011**, *32*, 5417−5426.
(9) Upadhyay, K. K.; Bhatt, A. N.; Mishra, A. K.; Dwarakanath, B. S.; Jain, S.; Schatz, C.; Le Meins, J. F.; Farooque, A.; Chandraiah, G.; Jain, A. K.; Misra, A.; Lecommandoux, S. The Intracellular Drug Delivery and Anti-tumor Activity of Doxorubicin Loaded Poly(γ-benzyl l-glutamate)-*b*-hyaluronan Polymersomes. *Biomaterials* **2010**, *31*, 2882−2892.
(10) Youns, M.; Hoheisel, J. D.; Efferth, T. Therapeutic and Diagnostic Applications of Nanoparticles. *Curr. Drug. Targets.* **2011**, *12*, 357−365.
(11) Dufes, C.; Muller, J. M.; Couet, W.; Olivier, J. C.; Uchegbu, I. F.; Schatzlein, A. G. Anticancer Drug Delivery with Transferrin Targeted Polymeric Chitosan Vesicles. *Pharm. Res.* **2004**, *21*, 101−107.
(12) Feng, X. L.; Lv, F. T.; Liu, L. B.; Tang, H. W.; Xing, C. F.; Yang, Q.; Wang, S. Conjugated Polymer Nanoparticles for Drug Delivery and Imaging. *ACS Appl. Mater. Interfaces* **2010**, *2*, 2429−2435.
(13) Sun, C. Y.; Ma, Y. C.; Cao, Z. Y.; Li, D. D.; Fan, F.; Wang, J. X.; Tao, W.; Yang, X. Z. Effect of Hydrophobicity of Core on the Anticancer Efficiency of Micelles as Drug Delivery Carriers. *ACS Appl. Mater. Interfaces* **2014**, *6*, 22709−22718.
(14) Maeda, H. The Enhanced Permeability and Retention (EPR) Effect in Tumor Vasculature: The Key Role of Tumor-Selective Macromolecular Drug Targeting. *Adv. Enzyme Regul.* **2001**, *41*, 189−207.
(15) Maeda, H.; Bharate, G. Y.; Daruwalla, J. Polymeric Drugs for Efficient Tumor-targeted Drug Delivery Based on EPR-effect. *Eur. J. Pharm. Biopharm.* **2009**, *71*, 409−419.
(16) Maeda, H.; Greish, K.; Fang, J. The EPR Effect and Polymeric Drugs: a Paradigm Shift for Cancer Chemotherapy in the 21st Century. *Polymer Therapeutics II*; Advances in Polymer Science; Springer, 2006; Vol. *193*, pp 103−121.
(17) Farokhzad, O. C.; Langer, R. Impact of Nanotechnology on Drug Delivery. *ACS Nano* **2009**, *3*, 16−20.
(18) Goldenbogen, B.; Brodersen, N.; Gramatica, A.; Loew, M.; Liebscher, J.; Herrmann, A.; Egger, H.; Budde, B.; Arbuzova, A. Reduction-Sensitive Liposomes from a Multifunctional Lipid Conjugate and Natural Phospholipids: Reduction and Release Kinetics and Cellular Uptake. *Langmuir* **2011**, *27*, 10820−10829.
(19) Kataoka, K.; Harada, A.; Nagasaki, Y. Block Copolymer Micelles for Drug Delivery: Design, Characterization and Biological Significance. *Adv. Drug Delivery Rev.* **2001**, *47*, 113−131.
(20) Chen, Y.; Ai, K. L.; Liu, Y. L.; Lu, L. H. Tailor-made Charge-Conversional Nanocomposite for pH-Responsive Drug Delivery and Cell Imaging. *ACS Appl. Mater. Interfaces* **2014**, *6*, 655−663.
(21) Secret, E.; Kelly, S. J.; Crannell, K. E.; Andrew, J. S. Enzyme-Responsive Hydrogel Microparticles for Pulmonary Drug Delivery. *ACS Appl. Mater. Interfaces* **2014**, *6*, 10313−10321.
(22) Cerritelli, S.; Velluto, D.; Hubbell, J. A. PEG-SS-PPS: Reduction-Sensitive Disulfide Block Copolymer Vesicles for Intracellular Drug Delivery. *Biomacromolecules* **2007**, *8*, 1966−1972.
(23) Yuan, Y. Y.; Liu, B. *ACS.* Self-Assembled Nanoparticles Based On Pegylated Conjugated Polyelectrolyte and Drug Molecules for Image-Guided Drug Delivery and Photodynamic Therapy. *ACS Appl. Mater. Interfaces* **2014**, *6*, 14903−14910.
(24) Takae, S.; Miyata, K.; Oba, M.; Ishii, T.; Nishiyama, N.; Itaka, K.; Yamasaki, Y.; Koyama, H.; Kataoka, K. PEG-detachable Polyplex Micelles Based on Disulfide-linked Block Catiomers as Bioresponsive Nonviral Gene Vectors. *J. Am. Chem. Soc.* **2008**, *130*, 6001−6009.
(25) Shao, Y.; Shi, C. Y.; Xu, G. F.; Guo, D. D.; Luo, J. T. Photo and Redox Dual Responsive Reversibly Cross-linked Nanocarrier for Efficient Tumor-Targeted Drug Delivery. *ACS Appl. Mater. Interfaces* **2014**, *6*, 10381−10392.
(26) Prabaharan, M.; Grailer, J. J.; Pilla, S.; Steeber, D. A.; Gong, S. Amphiphilic Multi-arm-block Copolymer Conjugated with Doxorubicin via pH-Sensitive Hydrazone Bond for Tumor-Targeted Drug Delivery. *Biomaterials* **2009**, *30*, 5757−5766.
(27) Song, E.; Han, W. Y.; Li, C.; Cheng, D.; Li, L. R.; Liu, L. C.; Zhu, G. Z.; Song, Y.; Tan, W. H. Hyaluronic Acid-Decorated Graphene Oxide Nanohybrids as Nanocarriers for Targeted and pH-Responsive Anticancer Drug Delivery. *ACS Appl. Mater. Interfaces* **2014**, *6*, 11882−11890.
(28) Lu, D. X.; Wen, X. T.; Liang, J.; Gu, Z. W.; Zhang, X. D.; Fan, Y. J. A PH-Sensitive Nano Drug Delivery System Derived from Pullulan/Doxorubicin Conjugate. *J. Biomed. Mater. Res., Part B* **2009**, *89*, 177−183.
(29) Mizrahy, S.; Peer, D. Polysaccharides as Building Blocks for Nanotherapeutics. *Chem. Soc. Rev.* **2012**, *41*, 2623−2640.
(30) Guhagarkar, S. A.; Gaikwad, R. V.; Samad, A.; Malshe, V. C.; Devarajan, P. V. Polyethylene Sebacate−Doxorubicin Nanoparticles for Hepatic Targeting. *Int. J. Pharm.* **2010**, *401*, 113−122.
(31) Yim, H.; Yang, S. G.; Jeon, Y. S.; Park, I. S.; Kim, M.; Lee, D. H.; Bae, Y. H.; Na, K. The Performance of Gadolinium Diethylene Triamine Pentaacetate-Pullulan Hepatocyte-Specific $T_1$ Contrast Agent for MRI. *Biomaterials* **2011**, *32*, 5187−5194.
(32) Rekha, M. R.; Sharma, C. P. Blood Compatibility and *in Vitro* Transfection Studies on Cationically Modified Pullulan for Liver Cell Targeted Gene Delivery. *Biomaterials* **2009**, *30*, 6655−6664.
(33) Trere, D.; Fiume, L.; De Giorgi, L. B.; Di Stefano, G.; Migaldi, M.; Derenzini, M. The Asialoglycoprotein Receptor in Human Hepatocellular Carcinomas: Its Expression on Proliferating Cells. *Br. J. Cancer.* **1999**, *81*, 404−408.
(34) Kunath, K.; von Harpe, A.; Fischer, D.; Kissel, T. Galactose-PEI-DNA Complexes for Targeted Gene Delivery: Degree of Substitution Affects Complex Size and Transfection Efficiency. *J. Controlled Release* **2003**, *88*, 159−172.
(35) David, A.; Kopecková, P.; Kopecek, J.; Rubinstein, A. The Role of Galactose, Lactose, and Galactose Valency in the Biorecognition of N-(2-Hydroxypropyl)Methacrylamide Copolymers by Human Colon Adenocarcinoma Cells. *Pharm. Res.* **2002**, *19*, 1114−1122.
(36) Ménard-Moyon, C.; Kostarelos, K.; Prato, M.; Bianco, A. Functionalized Carbon Nanotubes for Probing and Modulating Molecular Functions. *Chem. Biol.* **2010**, *17*, 107−115.
(37) Li, H. N.; Bian, S. Q.; Huang, Y. H.; Liang, J.; Fan, Y. J.; Zhang, X. D. High Drug Loading pH-sensitive Pullulan-DOX Conjugate Nanoparticles for Hepatic Targeting. *J. Biomed. Mater. Res., Part A* **2014**, *102*, 150−159.
(38) Bae, Y.; Jang, W. D.; Nishiyama, N.; Fukushima, S.; Kataoka, K. Multifunctional Polymeric Micelles with Folate-Mediated Cancer Cell Targeting and pH-Triggered Drug Releasing Properties For Active Intracellular Drug Delivery. *Mol. BioSyst.* **2005**, *1*, 242−250.
(39) *Pharmacopoeia of the People's Republic of China*; People's Medical Publishing House: 2005; Appendix 75−78.


DOI: 10.1021/acsami.5b03150
*ACS Appl. Mater. Interfaces* 2015, 7, 15855−15865